Nanoscale Advances

PAPER

View Article Online
View Journal | View Issue

Cite this: *Nanoscale Adv.*, 2019, **1**, 4989

Nano-SiO_2 coating enabled uniform Na stripping/plating for dendrite-free and long-life sodium metal batteries†

Fuyi Jiang,[a] Tianjiao Li,[a] Peng Ju,[b] Jianchao Sun, *[a] Chuang Liu,[a] Yiwei Li,[a] Xueqin Sun*[a] and Chengcheng Chen[c]

Received 17th October 2019
Accepted 16th November 2019

DOI: 10.1039/c9na00658c

rsc.li/nanoscale-advances

Metallic sodium, which has a suitable redox potential and high theoretical capacity, is regarded as an ideal anode material for rechargeable Na metal batteries. However, dendrite growth on sodium metal during cycling has seriously restricted its practical applications. Herein, we employed a low-cost and facile brushing method to fabricate a porous nano-SiO_2 coating, which can induce a relatively uniform distribution of Na^+ flux and suppress the growth of Na dendrites. The nano-SiO_2 coating with high porosity can decrease the Na stripping/plating overpotential (<50 mV) over 400 cycles at 5 mA cm^{-2}. Moreover, when coupled with a $Na_3V_2(PO_4)_3$ (NVP) cathode, the Na with SiO_2 coating (Na@SiO_2) composite anode shows a favorable suitability in a full cell. Compared with the one with a bare Na anode, the full cell with the Na@SiO_2 anode delivers a 27.8% higher discharge capacity (94.6 *vs.* 74 mA h g^{-1} at 1C) after 1000 cycles.

Introduction

Nowadays, as fossil fuel-related energy is consumed excessively and environmental awareness boosts, the demand for alternative clean energy is becoming more and more urgent.[1–4] Over the past few decades, rechargeable lithium-ion batteries (LIBs) have dominated portable electronics, medical microelectronics, and electric vehicles (EVs) as one of the most promising energy storage systems.[5–9] However, with the increasing demand for LIBs and shortage of lithium resources, the cost of lithium raw materials has increased rapidly.[10–12] Therefore, researching and exploring substitutes for LIBs has become one of the significant directions in the development of rechargeable batteries.[13–15] Because of the abundant reserves, low cost, and suitable electrochemical potential of Na, rechargeable Na batteries have received widespread attention and are regarded as the most promising substitute to LIBs.[16–20] However, some serious problems have hampered the practical application of rechargeable Na batteries.[21] The charge and Na^+ distribution on the surface of sodium metal are non-uniform during continuous charge–discharge cycling, resulting in the formation of sodium dendrites.[22,23] The dendrites not only affect the capacity and life of batteries, but cause safety problems such as short-circuits and explosions, hindering the practical application of sodium metal batteries (SMBs).[24,25] Therefore, solving the problem of Na metal dendrites generated during charge–discharge cycling is the key to improving the cycling stability and accelerating the commercial application of Na metal anodes.[26]

Recently, many methods have been adopted to restrain dendritic Na formation, including (1) the stabilization of the SEI layer by electrolyte modification;[27–29] (2) engineering artificial SEI layers by surface modification;[30–32] and (3) engineering nanostructured current collectors and hosts by artificial manufacture.[33–35] For instance, Wang and co-workers designed potassium bis(trifluoromethylsulfonyl)-imide (KTFSI) as a bifunctional electrolyte additive to stabilize the Na metal electrode.[36] In the work reported by Sun's group, an ultrathin protective coating was constructed as a protective layer on a Na metal anode through the ALD technique.[21] Luo' group stabilized Na metal anodes by employing a porous Al current collector as the plating substrate.[37] Hu and co-workers manufactured a stable Na-carbonized wood composite anode as a 3D host for Na metal.[38] These strategies provide insights for Na metal protection and achieve excellent electrochemical performance. Unfortunately, the expensive and complex preparation process poses substantial obstacles to the practical application of these strategies. Recently, Chen and Kang's group have designed nano-Super P and nano-$CaCO_3$ coatings respectively, which restrain the growth of Li and Zn dendrites.[39,40] Inspired by this, we explored a low-cost, simple, safe and scalable strategy to

[a]*School of Environment and Materials Engineering, Yantai University, Yantai, Shandong 264005, China. E-mail: jianchaoabc@163.com; sxq@ytu.edu.cn*

[b]*Key Laboratory of Marine Bioactive Substances and Analytical Technology, Marine Ecology Center, First Institute of Oceanography, Ministry of Natural Resources (MNR), Qingdao, Shandong 266061, China*

[c]*Key Laboratory of Advanced Energy Materials Chemistry (Ministry of Education), College of Chemistry, Nankai University, Tianjin 300071, China*

† Electronic supplementary information (ESI) available. See DOI: 10.1039/c9na00658c

inhibit the growth of non-uniform dendrites in the Na metal anode.

Herein, we report a simple method to construct a porous nano-SiO_2 coating as an auxiliary layer for inhibiting the growth of Na dendrites. We found that the nano-SiO_2 coating with a high porosity can be easily permeated by electrolyte. Compared with the bare Na anode (Fig. 1a), the Na anode with the SiO_2 coating induces a relatively uniform distribution of Na^+ flux (Fig. 1b).

The SiO_2 coating on the surface of Na acted as an electrolyte transport channel (like pores in water-permeable bricks), effectively dispersing Na^+ flux and achieving the purpose of suppressing dendrites. Consequently, the Na@SiO_2 composite electrode used in symmetrical cells exhibited excellent cycling stability with significantly reduced polarization. Furthermore, Na dendrites were found to be absent in the Na@SiO_2 electrode even at a current density of 5 mA cm^{-2} after 100 cycles. Moreover, we also tested a Na metal electrode with Super P coating, clearly finding that insulation coating (SiO_2) has advantages over conductive coating (Super P). Finally, we successfully constructed a full cell with an NVP cathode and a Na@SiO_2 anode, proving the benefits of this coating strategy for potential applications.

Experimental

Fabrication of Na@SiO_2 and Na@Super P electrodes

Firstly, a certain amount of nano SiO_2 or Super P was dried in a vacuum oven at 60 °C for 10 hours. Then, a Na disk (12 mm in diameter, 0.3 mm in thickness) was evenly coated with a SiO_2 or Super P layer (~100 μm) *via* brushing and rolling in an Ar-filled glovebox, and the mass loading of the layer is about 4.4 mg cm^{-2}.

Structural characterization

A scanning electron microscope (SEM, JSM-7610F) with an EDX attachment was used for obtaining SEM images and the corresponding EDX mapping images. For observing the morphology of electrodes after cycling, batteries were first disassembled in a glovebox and then the electrodes were rinsed with diglyme to remove residual Na salts. XRD patterns were obtained using a Rigaku D/MAX 2500/PC diffractometer with Cu Kα radiation (λ = 0.154 nm). Noticeably, the Na samples for SEM tests were loaded in a sealing device and covered with Kapton tape to avoid direct contact with air.

Electrochemical measurements

To investigate the electrochemical properties of Na stripping/plating, symmetrical 2032-type coin cells were assembled with two identical electrodes, which were either Na@SiO_2 or bare Na electrodes. For the preparation of the NVP cathode, NVP powder was mixed with carbon black and polyvinylidene fluoride (weight ratio of 8 : 1 : 1) using *N*-methyl-2-pyrrolidone as the solvent. The mass loading of the NVP cathode is about 1 mg. The electrolyte solution was 1 M sodium hexafluorophosphate ($NaPF_6$) in diglyme. All batteries were assembled in an argon-filled glovebox using the same dose of electrolyte (50 μL), and Celgard membrane was used as the separator. The batteries were first left to stand for four hours to stabilize the interface before tests. Galvanostatic cycling was carried out on a standard battery tester (Neware CT-4008-5 V/10 mA). EIS and CV were conducted on an electrochemical workstation. CV was performed in the potential window from 2.5 to 3.8 V at a scan rate of 0.1 mV s^{-1}.

Results and discussion

We employed a low-cost and facile brushing method to fabricate the Na@SiO_2 composite electrode. The hydrophobic SiO_2 used in this experiment is amorphous and the particle size is about 15 nm (Fig. S1†). Fig. 2a shows an optical photo and SEM image of a bare Na electrode, revealing a smooth, flat and shiny metallic surface. After brushing the nano SiO_2, the surface of Na was evenly coated with a white layer of spherical nano-SiO_2 particles (inset in Fig. 2b). Clearly, the fresh nano-SiO_2 coating is highly porous (Fig. 2b), which promotes electrolyte diffusion and ion migration in nano-channel pores.[41–45] Due to the high viscosity of Na, the nano-SiO_2 particles are tightly attached to

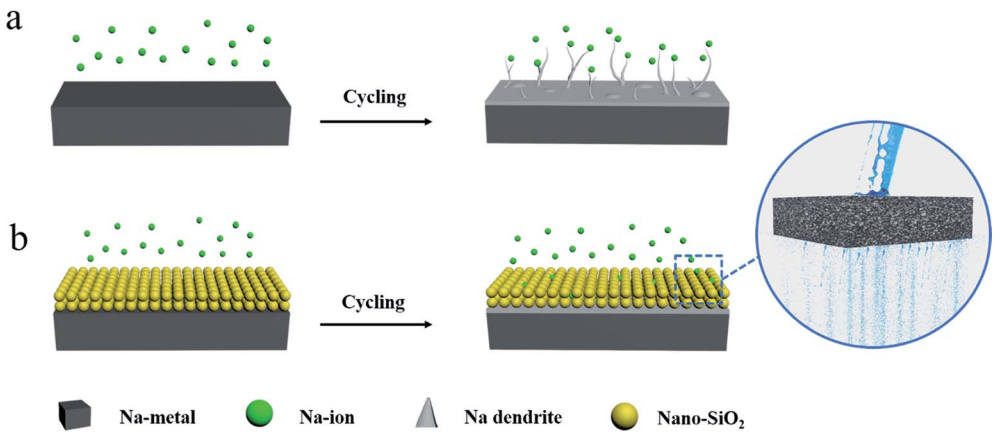

Fig. 1 Schematic illustrations of the Na stripping/plating behavior on (a) bare and (b) nano SiO_2 coated Na electrodes.

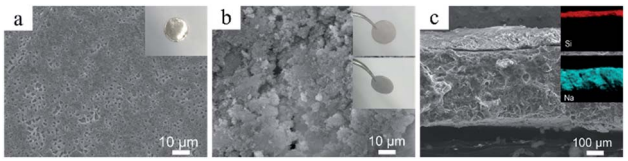

Fig. 2 The characterization of Na and Na@SiO_2 electrodes. (a) Top-view SEM image of a bare Na electrode and the corresponding digital image (inset). (b) Top-view SEM image of the Na@SiO_2 electrode, and the corresponding top and side view digital images (insets). (c) Cross-sectional SEM image of the Na@SiO_2 electrode and the corresponding EDX elemental mapping images of Si and Na (insets).

the metal surface and will not fall off when the Na@SiO_2 electrode is inverted with tweezers (insets in Fig. 2b). As shown in Fig. 2c, the thickness of the nano-SiO_2 coating is about 100 μm, which can be confirmed by EDX elemental mapping.

To assess the electrochemical performance of the Na@SiO_2 electrode, symmetric cells with two identical Na@SiO_2 electrodes were assembled in 1 M $NaPF_6$/diglyme electrolyte. For comparison, symmetric cells with two identical bare Na electrodes (thickness of ~300 μm) were assembled.

Fig. 3a shows the galvanostatic cycling performance of symmetric cells with Na@SiO_2 (yellow lines) and bare Na electrodes (green lines), respectively, for 400 cycles with a capacity of 1 mA h cm^{-2} at 1, 3 and 5 mA cm^{-2}. The symmetric cell with Na@SiO_2 electrodes exhibited stable voltage profiles and much lower hysteresis (5 mV) than the one with bare Na electrodes at 1 mA cm^{-2}. The bare Na electrode displayed a gradual increase in hysteresis (>25 mV), where the overpotential increases first, and then irregularly fluctuates, indicating a micro-short circuit.[46] When the current density was increased to 3 mA cm^{-2}, the Na@SiO_2 electrode still exhibited a small overpotential (15 mV) and very stable voltage profiles. In comparison, the symmetric cells with bare Na electrodes showed an anomalistic and apparently fluctuating voltage (>140 mV). As the current density was further increased to 5 mA cm^{-2}, the symmetrical cell with the bare Na electrode had large voltage polarization (>180 mV) and obviously poor stability, which is due to the uneven plating/stripping of Na metal, leading to the formation of dendrites. In contrast, the cell with the Na@SiO_2 electrode not only exhibited a much lower polarization (50 mV) but also realized very stable cycling under the same conditions. Furthermore, the rate behavior of the symmetric cells with bare Na and Na@SiO_2 electrodes is presented in Fig. 3b. As the current density increased from 0.5 to 10 mA cm^{-2}, the voltage polarization of the bare Na electrode increased greatly and tended to be unstable, which was attributed to irregular growth of Na dendrites on the electrode surface. Unfortunately, when the current density returned to 0.5 mA cm^{-2}, the battery no longer returned to its previous state, indicating poor cycling stability. In contrast, the cell using the Na@SiO_2 electrode continued to cycle steadily to 10 mA cm^{-2}. It is worth mentioning that when the current density returned to 0.5 mA cm^{-2}, the voltage profile was as stable as it was initially. To further demonstrate the superiority of the Na@SiO_2 electrode, higher capacity cycling of the symmetrical cell was performed and the results are

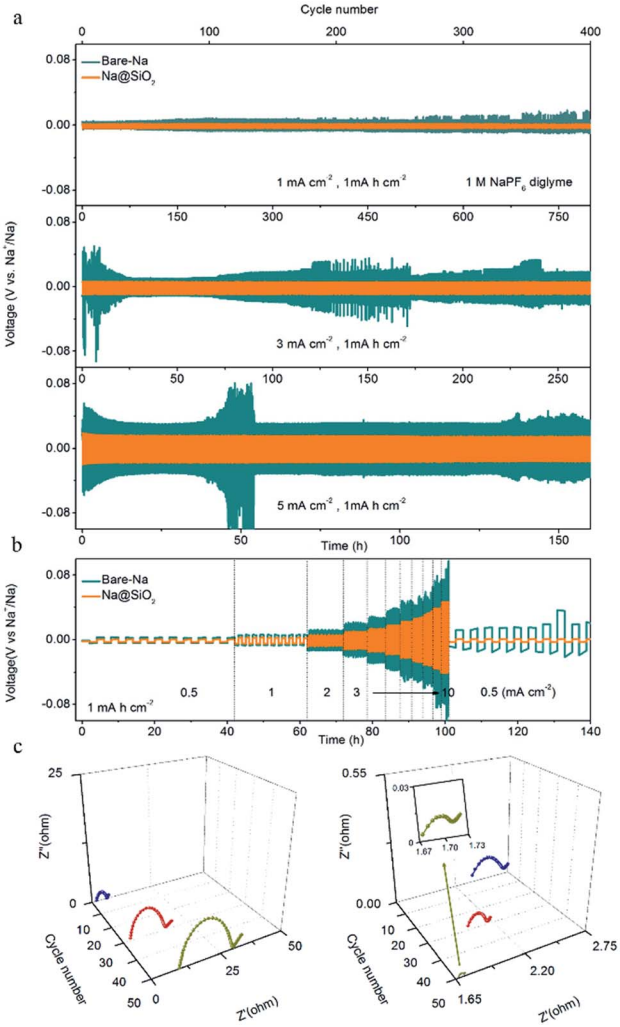

Fig. 3 Electrochemical performance of the Na@SiO_2 electrode. (a) Comparison of cycling stability of bare Na (green) and Na@SiO_2 electrodes (orange) in symmetrical cells at current densities of 1, 3 and 5 mA cm^{-2} with a capacity of 1 mA h cm^{-2}. (b) Rate performance. (c) EIS plots of bare Na (left) and Na@SiO_2 electrodes (right) in symmetrical cells after different cycles at a current density of 1 mA cm^{-2} with a capacity of 1 mA h cm^{-2}.

presented in Fig. S2.† The result demonstrated that the stability of the Na@SiO_2 electrode is significantly improved in virtue of the nano-SiO_2 coating, which could induce a relatively uniform distribution of Na^+ flux over the entire Na surface.[26,45,47]

Moreover, electrochemical impedance spectroscopy (EIS) was performed after 1, 30, and 50 cycles at a current density of 1 mA cm^{-2}. The interfacial resistance of the SEI and surface charge transfer impedance of the electrode were estimated according to the diameter of the semicircle in the high frequency range.[26,48] As shown in Fig. 3c, the Nyquist plots of the bare Na electrode show that the interface resistance increases after cycling (19 Ω in the 1st cycle, 25 Ω in the 30th cycle, and 35 Ω in the 50th cycle). This phenomenon is explained by the morphological transformation of the bare Na surface, indicating the occurrence of fractures in the SEI layer and the obvious growth of Na dendrites,[26] which is proven in the

subsequent SEM images. In addition, the ontological impedance of the symmetric cells with bare Na increases as the number of cycles increases, which is due to the generation of a large amount of non-conductive material during repeated repair of the SEI layer process, thereby degrading the overall conductivity of the battery.[49] The Na@SiO_2 electrode exhibited a smaller semicircle after cycling, indicating that the charge transfer resistance of the Na@SiO_2 composite electrode is much lower than that of bare Na. This could be attributed to the fact that the porous nano-SiO_2 coating induced a relatively uniform distribution of Na^+ flux and a stable SEI layer was formed on the Na metal electrode surface, thereby achieving the purpose of suppressing the generation of Na dendrites.[50]

The morphological evolution of bare Na and Na@SiO_2 electrodes after 100 cycles is shown in Fig. 4. The bare Na electrode exhibited a rough surface with rugged and mossy Na deposition at a current density of 1 mA cm^{-2} (Fig. 4a), which differed from the fresh Na electrode morphology. When the current density was increased to 3 and 5 mA cm^{-2}, the bare Na electrode showed an extremely inhomogeneous surface with excessive Na dendrites and dead Na (Fig. 4b and c). The morphological variation is mainly caused by the non-uniform Na plating/stripping and high reaction kinetics on the surface of sodium metal. In contrast, the morphology of the Na@SiO_2 electrode retained a flat surface without any detectable protrusions (Fig. 4d–f), which is attributed to the porous nano-SiO_2 coating for homogenizing the distribution of Na^+ on the Na surface. The above morphological evolution results demonstrate the role of nano-SiO_2 coating in restraining Na dendritic growth.

In order to further study the deposition behavior of Na on the Na@SiO_2 electrode, we further tested the Na metal electrode with conductive Super P coating (Na@Super P). The Super P used in this experiment is amorphous and the particle size is about 30 nm (Fig. S3†). The thickness of the Super P coating is about 100 μm (Fig. S4†). The electrodes with SiO_2 and Super P coatings all present small wetting angles (Fig. S5†), demonstrating excellent electrolyte permeability. Although both the SiO_2 layer and Super P layer are porous coatings, in terms of electrochemical properties, the latter has lower cycling stability than the former (Fig. 5a). The symmetric cells with the Na@Super P electrodes exhibited larger voltage hysteresis after 55 h. As shown in Fig. 5b, no Na metal was found on the surface of the SiO_2 coating after 50 cycles. We further proved that sodium metal was deposited at the bottom of the nano-SiO_2 coating layer after battery cycling by a cross-sectional SEM test (Fig. S6†). However, Na metal appeared on the surface of the Na@Super P electrodes after 50 cycles (Fig. 5c). The surface of the bare Na electrode is no longer flat after 100 cycles (Fig. S7a†), which is due to the formation of dendrites. The Na@SiO_2 electrode is almost unchanged (Fig. S7b†), while the Na@Super P electrode has changed from black to a metallic luster (Fig. S7c†). The high conductivity of the Super P layer may weaken the position limiting ability on Na electrodeposition, leading to preferential deposition of Na above the conductive coating rather than below it.[40] In contrast, owing to its electrically insulating properties, there should be a large variation of potential across the nano-SiO_2 coating.[51] Therefore, only the potential close to the surface of Na was low, and it was low enough for Na^+ to undergo a reduction reaction, forming a position-selective, bottom-up Na deposition process, instead of preferential deposition on Na protrusions/dendrite tips.[52]

To demonstrate the practical application of the Na@SiO_2 electrode, we further assembled full cells with bare Na or Na@SiO_2 as the anode and NVP as the cathode, respectively. The XRD profiles of NVP were consistent with PDF no. 70-3613 (Fig. S8a†). The SEM image indicates that the NVP particles are cross-linked with CNTs (Fig. S8b†).

A much higher NVP capacity was obtained with the Na@SiO_2 anodes during rate cycling (Fig. 6a). The NVP–Na@SiO_2 full cell exhibits superior capacities of 107, 99, 93, 89, 84, 80, 78, 76, 74

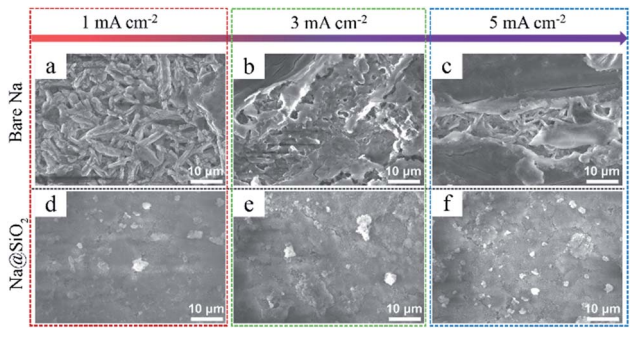

Fig. 4 Morphological evolution of bare Na and Na@SiO_2 electrodes after cycling. SEM images of (a–c) bare Na electrodes and (d–f) Na@SiO_2 electrodes after 100 stripping/plating cycles at different current densities, respectively. The current density is marked at the top of the figure and the stripping/plating capacity was 1 mA h cm^{-2}.

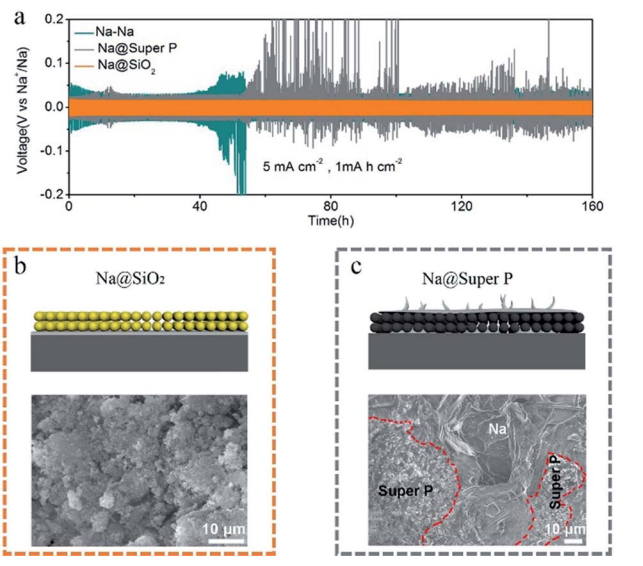

Fig. 5 (a) Comparison of the cycling stability of bare Na (green), Na@SiO_2 (orange) and Na@Super P (gray) electrodes at a current density of 5 mA cm^{-2} with a capacity of 1 mA h cm^{-2}. Schematic illustrations and SEM images of (b) Na@SiO_2 and (c) Na@Super P electrodes after 50 stripping/plating cycles at a current density of 5 mA cm^{-2} with a capacity of 1 mA h cm^{-2}.

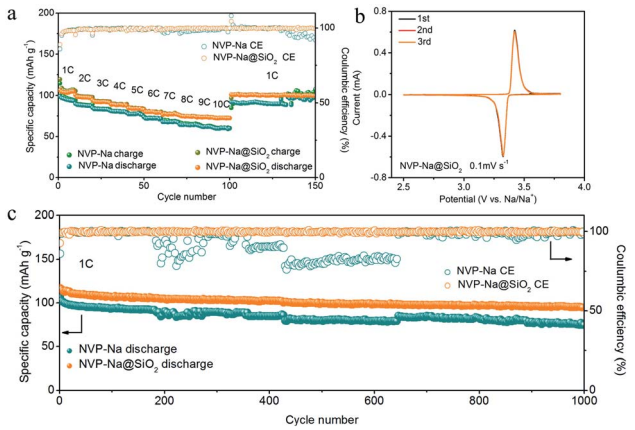

Fig. 6 Electrochemical performance of the full cells with bare Na or Na@SiO_2 as the anode and NVP as the cathode. (a) Rate capability of the NVP–Na and NVP–Na@SiO_2 cells at different rates from 1 to 10C (1C = 118 mA g^{-1}). (b) CVs of the NVP cathode at 0.1 mV s^{-1} coupled with the Na@SiO_2 anode. (c) Cycling stability of full cells with the bare Na or Na@SiO_2 anode at 1C, respectively.

and 72.5 mA h g^{-1} with the current density increasing from 1 to 10C (1C = 118 mA g^{-1}), respectively. After 150 consecutive cycles, a capacity of 106 mA h g^{-1} at 1C and an excellent coulombic efficiency of 99.4% are obtained. In contrast, the cells with bare Na anodes offer much lower capacities of 101, 89, 83, 80, 77, 72, 67, 64, 61 and 59 mA h g^{-1} with pronounced instability. Fig. 6b shows the cyclic voltammograms (CVs) of the NVP electrode, in which there are evident redox pairs at ~3.4 V. Furthermore, when galvanostatically cycled at 1C, the battery with the Na@SiO_2 anodes presented much better cycling stability than the one with bare Na anodes. As shown in Fig. 6c, it is observed that the cell with the Na@SiO_2 anode shows stable electrochemical performance (94.6 mA h g^{-1} after 1000 cycles, a capacity retention of 86.4%, and a coulombic efficiency of 99.8%). In sharp contrast, the cell with bare Na anodes exhibited a smaller initial discharge capacity of 100 mA h g^{-1}, and only retained 74 mA h g^{-1} after 1000 cycles with extremely unstable coulombic efficiency. The corresponding charge/discharge voltage–capacity profiles at the 1st and 500th cycles are shown in Fig. S9,† respectively. These results demonstrate the good adaptability of the Na@SiO_2 anode in full cells.

Conclusions

In conclusion, we developed a low-cost and simple brushing method to improve the stripping/plating stability of Na metal anodes. The porous nano-SiO_2 coating induces a relatively uniform distribution of Na^+ flux, resulting in uniform and dendrite-free deposition of metallic sodium. High cycling stability with low hysteresis was achieved in the Na@SiO_2 electrode even at a very high current density of 5 mA cm^{-2}. Furthermore, the Na@SiO_2|NVP full cell exhibits high cycling stability and superior suitability, making it far better than the full cell with bare Na as the anode. Our work provides an alternative route for the fabrication of safe Na metal anodes, which will be of great significance in the practical application of Na metal anodes for high-energy Na-based batteries.

Conflicts of interest

There are no conflicts of interest to declare.

Acknowledgements

This work was supported by the National Natural Science Foundation of China (51772257, 51702328 and 21805171), Major Basic Research Project of Shandong Natural Science Foundation (ZR2018ZC1459) and Shandong Natural Science Foundation (ZR2018BB038 and ZR2017BD002).

Notes and references

1 J. M. Tarascon and M. Armand, *Nature*, 2001, **414**, 359–367.
2 J. W. Choi and D. Aurbach, *Nat. Rev. Mater.*, 2016, **1**, 16013.
3 Y. Zhao, K. R. Adair and X. Sun, *Energy Environ. Sci.*, 2018, **11**, 2673–2695.
4 J. Sun, Y. Lu, H. Yang, M. Han, L. Shao and J. Chen, *Research*, 2018, **2018**, 6914626.
5 S. J. Tan, X. X. Zeng, Q. Ma, X. W. Wu and Y. G. Guo, *Electrochem. Energy Rev.*, 2018, **1**, 113–138.
6 J. Lu, Z. Chen, F. Pan, Y. Cui and K. Amine, *Electrochem. Energy Rev.*, 2018, **1**, 35–53.
7 G. Yang, H. Wang, B. Zhang, S. Foo, M. Ma, X. Cao, J. Liu, S. Ni, M. Srinivasan and Y. Huang, *Nanoscale*, 2019, **11**, 9556–9562.
8 Y. He, C. Lu, S. Liu, W. Zheng and J. Luo, *Adv. Energy Mater.*, 2019, **9**, 1901810.
9 S. Liu, L. Deng, W. Guo, C. Zhang, X. Liu and J. Luo, *Adv. Mater.*, 2019, **31**, 1807585.
10 A. Ponrouch, D. Monti, A. Boschin, B. Steen, P. Johansson and M. R. Palacín, *J. Mater. Chem. A*, 2015, **3**, 22–42.
11 D. Kundu, E. Talaie, V. Duffort and L. F. Nazar, *Angew. Chem., Int. Ed.*, 2015, **54**, 3431–3448.
12 X. Wang, L. Ma and J. Sun, *ACS Appl. Mater. Interfaces*, 2019, **11**, 41297–41303.
13 D. Aurbach, Z. Lu, A. Schechter, Y. Gofer, H. Gizbar, R. Turgeman, Y. Cohen, M. Moshkovich and E. Levi, *Nature*, 2000, **407**, 724–727.
14 Y. Liu, H. Kang, L. Jiao, C. Chen, K. Cao, Y. Wang and H. Yuan, *Nanoscale*, 2015, **7**, 1325–1332.
15 C. Chen, T. Li, H. Tian, Y. Zou and J. Sun, *J. Mater. Chem. A*, 2019, **7**, 18451–18457.
16 A. P. Cohn, N. Muralidharan, R. Carter, K. Share and C. L. Pint, *Nano Lett.*, 2017, **17**, 1296–1301.
17 K. Kretschmer, B. Sun, J. Zhang, X. Xie, H. Liu and G. Wang, *Small*, 2017, **13**, 1603318.
18 B. Xiao, H. Liu, J. Liu, Q. Sun, B. Wang, K. Kaliyappan, Y. Zhao, M. N. Banis, Y. Liu, R. Li, T.-K. Sham, G. A. Botton, M. Cai and X. Sun, *Adv. Mater.*, 2017, **29**, 1703764.
19 N. Yabuuchi, K. Kubota, M. Dahbi and S. Komaba, *Chem. Rev.*, 2014, **114**, 11636–11682.

20 R. Zhang, Y. Cui, W. Fan, G. He and X. Liu, *Electrochim. Acta*, 2019, **295**, 181–186.
21 Y. Zhao, L. V. Goncharova, A. Lushington, Q. Sun, H. Yadegari, B. Wang, W. Xiao, R. Li and X. Sun, *Adv. Mater.*, 2017, **29**, 1606663.
22 H. Tian, Z. W. Seh, K. Yan, Z. Fu, P. Tang, Y. Lu, R. Zhang, D. Legut, Y. Cui and Q. Zhang, *Adv. Energy Mater.*, 2017, **7**, 1602528.
23 W. Luo and L. Hu, *ACS Cent. Sci.*, 2015, **1**, 420–422.
24 R. D. D. I. Iermakova, M. R. Palacín and A. Ponrouch, *J. Electrochem. Soc.*, 2015, **166**, 7060–7066.
25 X. Li, L. Zhao, P. Li, Q. Zhang and M. Wang, *Nano Energy*, 2017, **42**, 122–128.
26 S. Chi, X. Qi, Y. Hu and L. Fan, *Adv. Energy Mater.*, 2018, **8**, 1702764.
27 N. Ingersoll, Z. Karimi, D. Patel, R. Underwood and R. Warren, *Electrochim. Acta*, 2019, **297**, 129–136.
28 J. Lee, Y. Lee, J. Lee, S. M. Lee, J. H. Choi, H. Kim, M. S. Kwon, K. Kang, K. T. Lee and N. S. Choi, *ACS Appl. Mater. Interfaces*, 2017, **9**, 3723–3732.
29 J. Zheng, S. Chen, W. Zhao, J. Song, M. H. Engelhard and J. Zhang, *ACS Energy Lett.*, 2018, **3**, 315–321.
30 Q. Liu, J. Xu, S. Yuan, Z. Chang, D. Xu, Y. Yin, L. Li, H. Zhong, Y. Jiang, J. Yan and X. Zhang, *Adv. Mater.*, 2015, **27**, 5241–5247.
31 W. Luo, C. Lin, O. Zhao, M. Noked, Y. Zhang, G. W. Rubloff and L. Hu, *Adv. Energy Mater.*, 2017, **7**, 1601526.
32 Y. Zhao, L. V. Goncharova, Q. Zhang, P. Kaghazchi, Q. Sun, A. Lushington, B. Wang, R. Li and X. Sun, *Nano Lett.*, 2017, **17**, 5653–5659.
33 J. Sun, C. Guo, Y. Cai, J. Li, X. Sun, W. Shi, S. Ai, C. Chen and F. Jiang, *Electrochim. Acta*, 2019, **309**, 18–24.
34 Y. Lu, Q. Zhang, M. Han and J. Chen, *Chem. Commun.*, 2017, **53**, 12910–12913.
35 H. J. Yoon, N. R. Kim, H. J. Jin and Y. S. Yun, *Adv. Energy Mater.*, 2018, **8**, 1701261.
36 Q. Shi, Y. Zhong, M. Wu, H. Wang and H. Wang, *Angew. Chem.*, 2018, **57**, 9069–9072.
37 S. Liu, S. Tang, X. Zhang, A. Wang, Q. Yang and J. Luo, *Nano Lett.*, 2017, **17**, 5862–5868.
38 W. Luo, Y. Zhang, S. Xu, J. Dai, E. Hitz, Y. Li, C. Yang, C. Chen, B. Liu and L. Hu, *Nano Lett.*, 2017, **17**, 3792–3797.
39 J. Wang, J. Liu, Y. Cai, F. Cheng, Z. Niu and J. Chen, *ChemElectroChem*, 2018, **5**, 1702–1707.
40 L. Kang, M. Cui, F. Jiang, Y. Gao, H. Luo, J. Liu, W. Liang and C. Zhi, *Adv. Energy Mater.*, 2018, **8**, 1801090.
41 H. Bian, J. Zhang, M. F. Yuen, W. Kang, Y. Zhan, D. Y. W. Yu, Z. Xu and Y. Y. Li, *J. Power Sources*, 2016, **307**, 634–640.
42 S. J. R. Prabakar, J. Jeong and M. Pyo, *Electrochim. Acta*, 2015, **161**, 23–31.
43 Y. Wang, H. Li, P. He, E. Hosono and H. Zhou, *Nanoscale*, 2010, **2**, 1294–1305.
44 C. Wang, A. Wang, L. Ren, X. Guan, D. Wang, A. Dong, C. Zhang, G. Li and J. Luo, *Adv. Funct. Mater.*, 2019, **29**, 1905940.
45 C. Wei, R. Zhang, X. Zheng, Q. Ru, Q. Chen, C. Cui, G. Li and D. Zhang, *Inorg. Chem. Front.*, 2018, **5**, 3126–3134.
46 X. Han, Y. Gong, K. Fu, X. He, G. T. Hitz, J. Dai, A. Pearse, B. Liu, H. Wang, G. Rubloff, Y. Mo, V. Thangadurai, E. D. Wachsman and L. Hu, *Nat. Mater.*, 2016, **16**, 572.
47 N. Muralidharan, A. P. Cohn, R. Carter, K. Share and C. L. Pint, *Nano Lett.*, 2017, **17**, 1296–1301.
48 D. Lin, Y. Liu, Z. Liang, H. W. Lee, J. Sun, H. Wang, K. Yan, J. Xie and Y. Cui, *Nat. Nanotechnol.*, 2016, **11**, 626.
49 J. Meng, F. Chu, J. Hu and C. Li, *Adv. Funct. Mater.*, 2019, **29**, 1902220.
50 X. Q. Zhang, X. Chen, X. B. Cheng, B. Q. Li, X. Shen, C. Yan, J. Q. Huang and Q. Zhang, *Angew. Chem., Int. Ed.*, 2018, **57**, 5301–5305.
51 K. N. Wood, E. Kazyak, A. F. Chadwick, K. H. Chen, J. G. Zhang, K. Thornton and N. P. Dasgupta, *ACS Cent. Sci.*, 2016, **2**, 790–801.
52 D. D. Joshua, W. Gallaway, A. Gaikwad, C. Corredor, S. Banerjee and D. Steingart, *J. Electrochem. Soc.*, 2010, **157**, 1279–1286.